

Estimation of the freeze-out parameters reachable in the AFTER@LHC project

Viktor Begun,^{1,*} Daniel Kikoła,^{1,†} Volodymyr Vovchenko,^{2,3,‡} and Daniel Wielanek^{1,§}

¹*Warsaw University of Technology, Faculty of Physics, Koszykowa 75, 00-662 Warsaw Poland*

²*Institut für Theoretische Physik, Goethe Universität Frankfurt, D-60438 Frankfurt am Main, Germany*

³*Frankfurt Institute for Advanced Studies, Giersch Science Center, D-60438 Frankfurt am Main, Germany*

(Dated: December 14, 2024)

Estimation of the freeze-out parameters as the function of rapidity in Pb+Pb collisions at $\sqrt{s_{NN}} = 72$ GeV in the AFTER@LHC project is performed. The conventional hadron resonance gas model is used for the analysis of the events generated by the UrQMD model. The results indicate that one may obtain at least 2.5 times increase of baryon chemical potential μ_B in the forward rapidity range as compared to the mid-rapidity. The μ_B values in the rapidity range of $0 < y < 4.5$ for AFTER@LHC is comparable to that covered by the RHIC Beam Energy Scan program. Thus, a rapidity scan in the AFTER@LHC project provides a complementary approach to study the QCD phase diagram.

PACS numbers:

Keywords: heavy-ion collisions, QCD phase diagram, rapidity scan, CERN LHC, AFTER@LHC, ALICE, LHCb

The determination of the phase structure of the strongly-interacting QCD matter is one of the most fundamental open questions in nuclear physics. The QCD phase diagram is usually expressed in terms of the temperature, T , and the baryon chemical potential, μ_B . The experimental data collected in high-energy heavy-ion collision experiments at the Super Proton Synchrotron (SPS), Relativistic Heavy-Ion Collider (RHIC) and the Large Hadron Collider (LHC) provide a strong evidence that a state of matter with partonic degrees of freedom (the Quark-Gluon Plasma, QGP) is created in such collisions [1–10]. The lattice QCD calculations indicate that there is a “smooth” phase transition between the hadronic matter and the QGP at $\mu_B = 0$, the so-called crossover transition [11–13]. Theory calculations suggest that at large μ_B range the 1st order phase transition takes place [14–18], thus the QCD critical point, that separates these two types of the phase transitions, is expected to exist. However, the corresponding theoretical calculations provide little guidance on the position of the critical point on the temperature and baryon chemical potential phase diagram - the predictions cover almost the whole $T(\mu_B)$ plane [19]. Therefore, the search for the critical point of the QCD matter is one of the main motivations for the ongoing and future experiments on heavy ion collisions (see, e.g., [20–25]).

The present experimental methods to change T and μ_B are either to vary the collision energy, or to change the types of colliding nuclei. However, such an approach has some significant constraints. The energies available are limited by the accelerator capabilities, see for example the RHIC Beam Energy Scan program phase I and II [21]. Thus, it is possible to miss the critical point in a collision energy scan. Moreover, the amount of the available statistics decreases significantly with decreasing bombarding energy in the collider mode. This limits the high-statistics studies to low transverse momenta and only to the most abundant particle species.

In this paper we recall the alternative approach: varying the rapidity interval at a fixed collision energy [26–30]. In a rapidity scan one compares subsystems corresponding to different rapidity bins, which can be characterized by different thermodynamic parameters. We provide estimates of the T and μ_B values reachable at different rapidities in a fixed target experiment at the LHC - the AFTER@LHC project [31] (see also [32]).

A fixed target experiment using TeV beams of the Large Hadron Collider exhibits a couple of unique features. Such an experiment will have a wide kinematic coverage. The collision of 2.76 TeV heavy-ion (for instance Pb) beam on a fixed target releases a center-of-mass-system (c.m.s.) energy of $\sqrt{s_{NN}} = 72$ GeV. These collisions occur in a frame with an extremely large Lorentz factor $\gamma \approx 4.3$. Due to the Lorentz boost, the forward instrumentation of existing LHC detectors provides a mid-rapidity coverage in the c.m.s. For example, the LHCb experiment with the pseudorapidity coverage of $2 < \eta < 5$ in the laboratory frame would cover the c.m.s. rapidity of $-2.3 \lesssim y \lesssim 0.7$. In the case of the ALICE experiment, the central detector (with $|y^{Lab}| < 0.9$) becomes a “backward” one in the fixed-target mode, with access to the large absolute value of rapidity in the c.m.s. with $-5.2 \lesssim y^{c.m.s.} \lesssim -3.4$. In general, AFTER@LHC will provide a broad kinematic coverage $-5.2 \lesssim y^{c.m.s.} \lesssim 0.7$, which is not the case in the collider mode. The available luminosity per year is very

*Electronic address: viktor.begun@gmail.com

†Electronic address: danie.kikola@pw.edu.pl

‡Electronic address: vlvovch@gmail.com

§Electronic address: daniel.wielanek@cern.ch

high, similar to the nominal LHC luminosities, and orders of magnitude larger than that at RHIC in the similar energy range [33]. Such amount of data gives access to rare probes like heavy quarks – quarkonium [34] and open heavy flavor hadrons. In addition, one can easily change the atomic mass of the target, which facilitate the system-size dependence study. In general the AFTER@LHC project will have a broad physics program which includes the high- x frontier, the spin physics at the LHC (given the installation of the polarized target) and the heavy-ion physics (see, e.g., [33, 35–38] and other publications and presentations at [31]). All of that can, in principle, be achieved in a cost effective way, by collecting data in the fixed-target mode in the existing experiments (LHCb and ALICE) in parallel to the collider-mode operation. For the study described in this paper, we assume that AFTER@LHC will deliver a sufficiently good particle identification over a broad rapidity range, an expectation based on the capabilities of the LHCb and the ALICE detectors. Moreover, the LHCb experiment has already proven that it is capable of registration and identification of particles, and performing physics measurements in a fixed-target mode [39].

We perform estimates of the temperature T , baryochemical potential μ_B and (rapidity slice) volume V of the system created in the AFTER@LHC in two steps. First, we calculate the mean multiplicities of produced particles using the UrQMD model [40, 41]. Second, we fit the obtained mean multiplicities in a hadron resonance gas (HRG) model. We use the UrQMD-3.4 model to generate the 10% most central Pb+Pb collisions at the $\sqrt{s_{NN}} = 72$ GeV. The number of events $N_{ev} \simeq 2 * 10^5$. The UrQMD is run in the cascade mode, without hydro, for simplicity. The resulting rapidity distribution for different hadron species is shown in Fig. 1, in steps of $\Delta y = 0.5$. The Δy step is chosen so that it is small enough to catch the forward rapidity increase of the

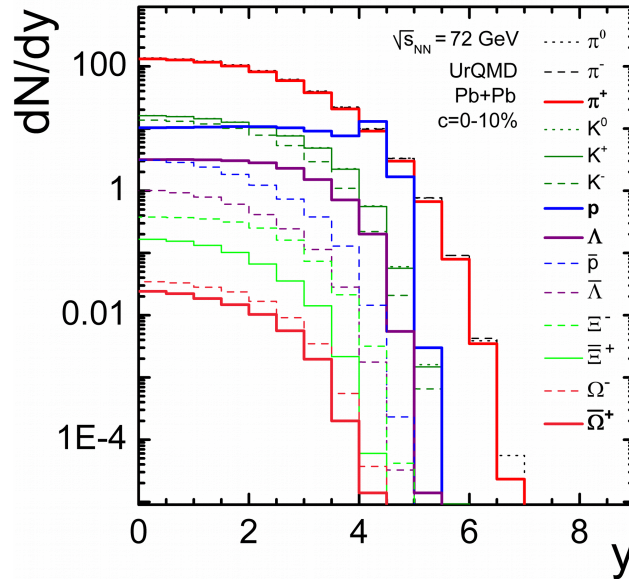


FIG. 1: Rapidity dependence of particle multiplicities per event generated in the UrQMD model. The order of particle labels is sorted according to their abundance at $y = 0$.

dN/dy for protons, but not too small so as to have enough statistics for the chosen particles. The increase in dN/dy for protons is very well seen in the data, see e.g. Refs. [42–45], and is reproduced by the UrQMD, see e.g. Refs. [46, 47]. The particle set is chosen in order to be able to constrain the HRG parameters in a thermal fit.

We use the same realization of a HRG model as in Refs. [48, 49]. A general description of HRG model can be found following Refs. [50–52]. For the recent applications of the HRG model see e.g. [53–55], and references therein. We consider only the grand canonical ensemble, thus, we imply that baryon number B , electric charge Q , and strangeness of the system, S , are conserved on average. Moreover, we assume no additional interactions between particles in a HRG, therefore excluded-volume [56–58] or van der Waals interaction effects [59] are omitted. This provides an internal consistency of the procedure since these interactions are presently omitted in UrQMD as well. We expect strangeness non-equilibrium in small dN/dy bins, therefore, we do include the γ_S parameter [60] into fits. Thus, we have six parameters in the HRG – the system temperature T , the three chemical potentials, μ_B , μ_Q , μ_S , the γ_s , and the radius of the system R . The radius parameter R characterizes the system volume as $V = (4/3)\pi R^3$. Two chemical potentials, μ_Q and μ_S , are constrained for each considered rapidity bin by the conditions of zero net strangeness, $\langle S \rangle = 0$, and by the ratio of electric charge to baryon charge of $\langle Q \rangle / \langle B \rangle \simeq 0.4$, as in a Pb nuclei. Thus, the number of free parameters is four – T , μ_B , γ_s , R .

The set of the input mean multiplicities should contain all three conserved charges, mesons, baryons, and their anti-particles. Therefore we choose the following particle set which satisfies these conditions: π^0 , π^\pm , K^0 , K^\pm , p , \bar{p} , Λ , $\bar{\Lambda}$, Ξ^- , Ξ^+ , Ω^- , $\bar{\Omega}^+$. The thermal fit requires both mean hadron yields and their uncertainties. The statistical uncertainty scales with the number of events as $1/\sqrt{N_{ev}}$, and becomes very small for a large number of generated events. We additionally assume a theoretical systematic relative uncertainty of 10% for the UrQMD yields. This makes the uncertainties comparable to the experimental ones in the RHIC BES program [61] or in the ALICE experiment [62, 63], where they are dominated by systematic uncertainties. where hadron yield data have about 10% uncertainty for each measured multiplicity. The output of the thermal fits is shown in Figs. 2, 3, 4. The uncertainties of the HRG parameters result from the assumed 10% uncertainties of the input multiplicities from UrQMD. The freedom in choosing the input uncertainties is the reason why we do not put too much focus on the magnitude of the χ^2 values. We do note that χ^2 values are smaller at small rapidities ($\chi^2/N_{dof} \sim 1$), and show a rapid increase for large ($y > 3$) rapidities.

Both T and μ_B are depicted as a function of rapidity in Figs. 2 and 3, respectively. The chemical freeze-out

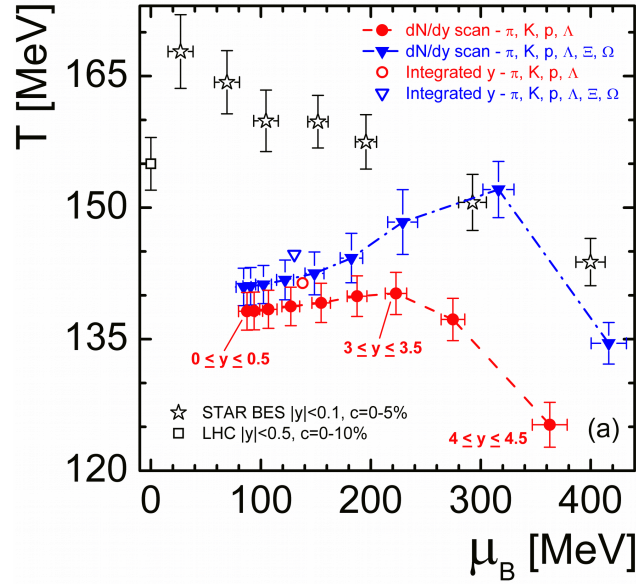


FIG. 2: The values of the T - μ_B pairs extracted from the thermal fits to the dN/dy UrQMD output (Fig. 1) for different rapidity slices are shown by the red/blue full symbols. The fits to the rapidity-integrated (4π) yields are shown by the open symbols. Also shown are the fits to STAR-BES [61] and ALICE [64] data (black open symbols).

temperature is approximately constant for the larger part of the rapidity interval (as is commonly assumed [26, 27]), but then drops at large rapidity (a behavior also seen in [28, 29]). The extracted temperature values do depend on the particle set. Adding heavy strange baryons leads to an increase in the extracted temperature. This effect is also seen in the fit of the real data by STAR [61]. We see that this dependence becomes even stronger in forward rapidities. The obtained temperature values are about 20 MeV smaller than the temperatures extracted from fits to the real data at RHIC and LHC. In that regard one should note that UrQMD contains string excitation and fragmentation, which results in a Hagedorn-like equation of state in box simulations [65, 66]. The temperature values that we observe, $T \sim 140$ MeV, appear to be caused by this property of the UrQMD model. Correcting for this UrQMD behavior, one arrives at $T \sim 150 - 160$ MeV as an estimate of the chemical freeze-out temperatures reached in the AFTER@LHC project.

The results for the μ_B appear to be much more reliable, in part because the UrQMD was constrained to the rapidity distributions at various energies [46]. The increase of μ_B with y is caused by the data driven increase of the baryon number dN/dy and by the decrease of the dN/dy for other particles at large y [42–45, 67].

A similar y -dependence of $\mu_B(y)$ was observed earlier at top RHIC energy of $\sqrt{s} = 200$ GeV [28, 29], where it was fitted with a parabola:

$$\mu_B(y) = a + by^2, \quad (1)$$

where the fit parameters were found to be $a = 25 - 26$ MeV and $b = 11 - 12$ MeV.

We perform a similar parabolic fit to the extracted y -dependence $\mu_B(y)$ at the AFTER@LHC energy (Fig. 3b). We obtain $a = 75.5 \pm 5.9$, $b = 16.6 \pm 1.0$ for the full particle set, and $a = 84.5 \pm 3.2$, $b = 13.9 \pm 0.5$ for the set

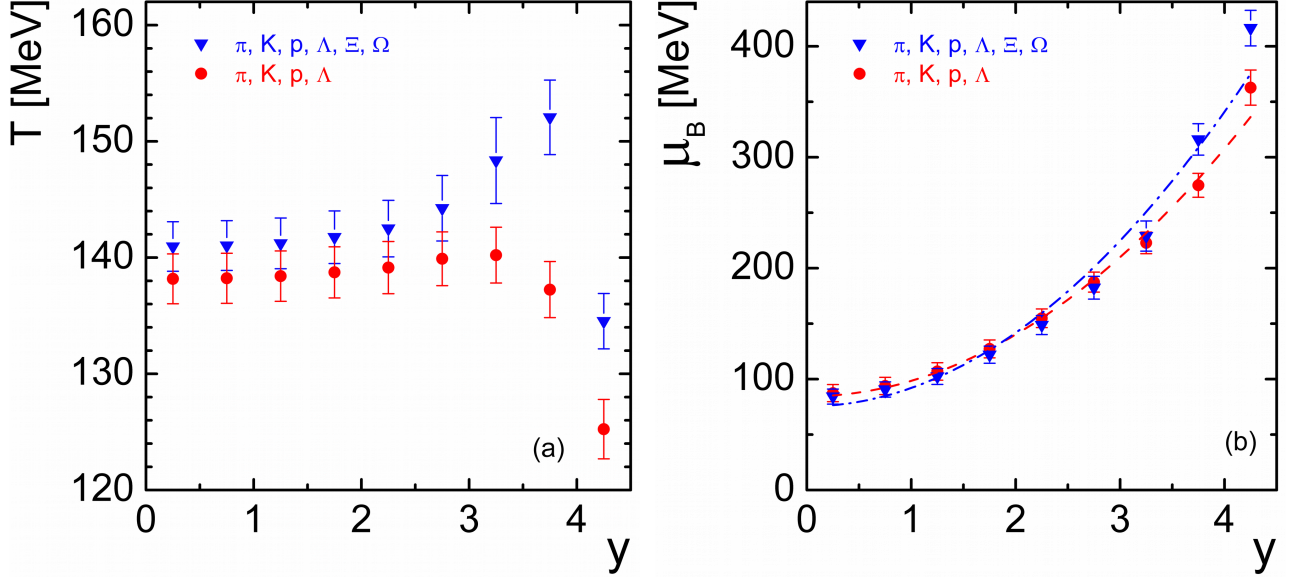


FIG. 3: The extracted chemical freeze-out temperature (a) and the baryon chemical potential (b) as the function of rapidity. The lines show the fit of the thermal fits output with a parabola.

without Ξ and Ω . The a parameter is larger than in [28, 29], because we study a smaller collision energy. The b parameter is similar, with an indication for the stronger increase of μ_B at large y .

Let us denote the rapidity range, $0 < y < 2.5$, as the “conservative” one, and the full considered rapidity range, $0 < y < 4.5$, as the “optimistic” one. The temperature in the “conservative” rapidity range is the same for both particle sets, while the μ_B changes by a factor 2.5. The change of the μ_B in the “optimistic” range is much higher - up to a factor of 4.5. The change of μ_B with rapidity can be expected to be even stronger in peripheral collisions, but also with a stronger dependence on the particle set used in fits etc. In that regard we stress that the goal of this paper is not the determination of the T and μ_B with an accuracy up to a few MeV, but rather to answer whether the rapidity scan can be used to change μ_B by the amount notably larger than the uncertainty of T and μ_B at midrapidity. Therefore, we limit our study only to the case of the most central collisions.

The radius parameter, R , and the strangeness undersaturation parameter, γ_S , behave as expected: they decrease with y , see Fig. 4. The values of R and γ_S are between the values obtained for the rapidity-integrated (4π) multiplicities measured in central Pb+Pb and p+p collisions at the SPS energies [48, 49]. The mid-rapidity values of R and γ_S resemble the Pb+Pb collisions, while forward rapidities resemble p+p. This is due to the fact that bulk of the particles are produced at mid-rapidity, and their dN/dy drops fast with increasing y , see Fig. 1. However, the radius parameter (i.e. the system volume) for the most forward considered rapidity bin is still much larger than that in p+p collisions, see [48, 49].

We have also performed fits to the rapidity-integrated (4π) UrQMD multiplicities. The corresponding system radius parameter for the full hadron set is $R = 9.73 \pm 0.46$, while for the set without Ξ and Ω the radius is $R = 10.54 \pm 0.48$. The fit of the 4π multiplicities gives the T - μ_B values close to those obtained from mid-rapidity fits, see open symbols in Fig. 2. This is expected since the bulk of hadron production is peaked at $y = 0$. The volume of the HRG system that we obtained from the fit to the 4π multiplicities, $V = 4898 \pm 672 \text{ fm}^3$ (no Ξ, Ω), $V = 3864 \pm 543 \text{ fm}^3$ (with Ξ, Ω). The sum of the volumes obtained from the fits for the rapidity sub-bins is $V = 5441 \pm 276 \text{ fm}^3$ for hadron set without Ξ, Ω , and $V = 4225 \pm 210 \text{ fm}^3$ for the full hadron set (with Ξ, Ω), these values agree with the 4π fit results within uncertainty. This indicates that the performed Δy binning is correct.

The luminosity available for Pb+Pb collisions at AFTER@LHC is large. The integrated luminosity is $L_{int} \sim 1.6 \text{ nb}^{-1}$ [33] per year, which corresponds to ≈ 11.5 billion minimum bias events. Given the particle yields predicted by the UrQMD, and assuming even a very conservative value of the reconstruction uncertainty of 1% [62, 68] in the ALICE detector, the measurement precision of all particle species (except for the heaviest and the infrequent $\bar{\Omega}$) yields over the whole rapidity range considered here will be limited only by the systematic uncertainties. Only the study of the $\bar{\Omega}$ baryon at the most forward rapidity bin could be a challenge, since the yield from the UrQMD model is low, and the success will depend on the $\Omega(\bar{\Omega})$ reconstruction efficiency

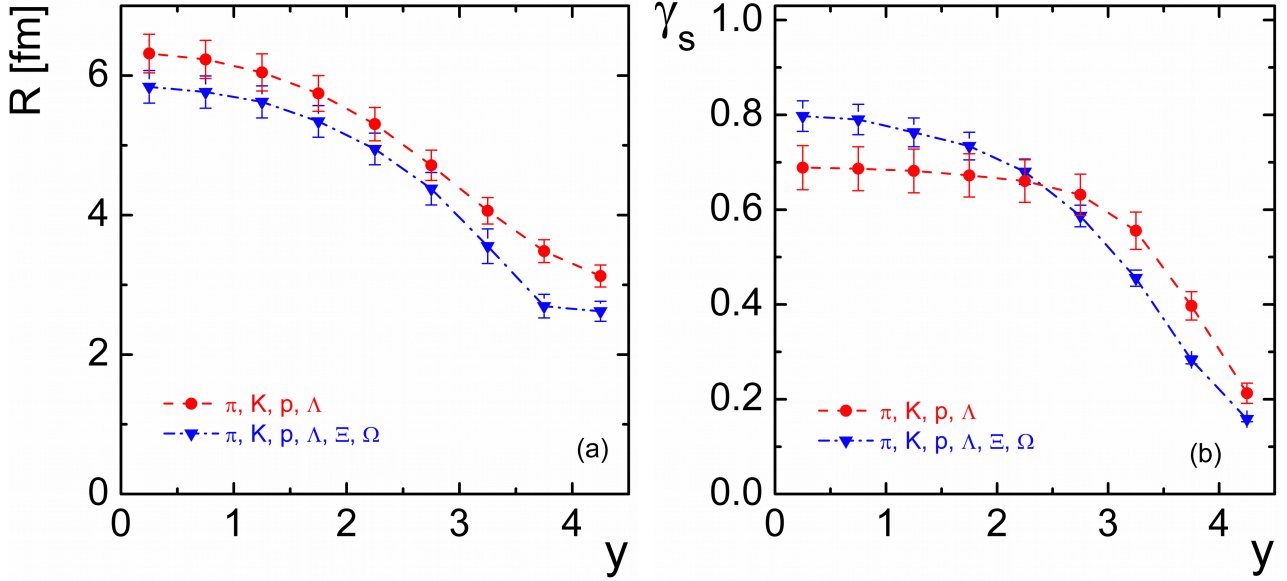


FIG. 4: The system radius parameter R (a), and the strangeness undersaturation parameter γ_s (b) as the function of rapidity.

available in the fixed-target mode. With a 4% reconstruction efficiency, and assuming the signal-to-background ratio of 3:1 [62] and the yield per event predicted by the UrQMD model, it will be possible to measure $\bar{\Omega}$ with 10% relative uncertainty. Thus, the studies proposed here are definitely within the reach of a single-year Pb+Pb program at the AFTER@LHC.

We conclude that the dN/dy scan with Pb+Pb collisions at the $\sqrt{s_{NN}} = 72$ GeV may deliver systems which have similar temperatures, but at least a factor 2.5 larger baryon chemical potential in forward rapidity compared to mid-rapidity. The rapidity scan at the AFTER@LHC covers the majority of the μ_B range accessible in the RHIC Beam Energy Scan program. Therefore, such a dN/dy study in the AFTER@LHC project will provide a complementary approach to the QCD phase diagram studies, but with all the benefits of a high-luminosity fixed-target experiment at the LHC.

Acknowledgments

The authors thank M. I. Gorenstein, K. Grebieszko for fruitful discussions. DK gratefully acknowledges inspiring discussions with Jean-Philippe Lansberg.

-
- [1] NA49, S. V. Afanasiev *et al.*, Phys. Rev. **C66**, 054902 (2002), nucl-ex/0205002.
 - [2] PHENIX, K. Adcox *et al.*, Nucl. Phys. **A757**, 184 (2005), nucl-ex/0410003.
 - [3] B. B. Back *et al.*, Nucl. Phys. **A757**, 28 (2005), nucl-ex/0410022.
 - [4] BRAHMS, I. Arsene *et al.*, Nucl. Phys. **A757**, 1 (2005), nucl-ex/0410020.
 - [5] STAR, J. Adams *et al.*, Nucl. Phys. **A757**, 102 (2005), nucl-ex/0501009.
 - [6] ALICE, B. B. Abelev *et al.*, JHEP **06**, 190 (2015), 1405.4632.
 - [7] ATLAS, G. Aad *et al.*, Phys. Lett. **B707**, 330 (2012), 1108.6018.
 - [8] ALICE, K. Aamodt *et al.*, Phys. Lett. **B696**, 30 (2011), 1012.1004.
 - [9] ATLAS, G. Aad *et al.*, Phys. Rev. Lett. **105**, 252303 (2010), 1011.6182.
 - [10] CMS, S. Chatrchyan *et al.*, Phys. Rev. **C84**, 024906 (2011), 1102.1957.
 - [11] Y. Aoki, G. Endrodi, Z. Fodor, S. D. Katz, and K. K. Szabo, Nature **443**, 675 (2006), hep-lat/0611014.
 - [12] S. Borsanyi *et al.*, JHEP **11**, 077 (2010), 1007.2580.
 - [13] A. Bazavov *et al.*, Phys. Rev. **D85**, 054503 (2012), 1111.1710.
 - [14] S. P. Klevansky, Rev. Mod. Phys. **64**, 649 (1992).
 - [15] A. Barducci, R. Casalbuoni, G. Pettini, and R. Gatto, Phys. Rev. **D49**, 426 (1994).

- [16] M. A. Stephanov, Phys. Rev. Lett. **76**, 4472 (1996), hep-lat/9604003.
- [17] M. G. Alford, K. Rajagopal, and F. Wilczek, Phys. Lett. **B422**, 247 (1998), hep-ph/9711395.
- [18] M. A. Stephanov, K. Rajagopal, and E. V. Shuryak, Phys. Rev. Lett. **81**, 4816 (1998), hep-ph/9806219.
- [19] M. A. Stephanov, Prog. Theor. Phys. Suppl. **153**, 139 (2004), hep-ph/0402115, [Int. J. Mod. Phys.A20,4387(2005)].
- [20] D. Keane, J. Phys. Conf. Ser. **878**, 012015 (2017).
- [21] The STAR Collaboration, Studying the Phase Diagram of QCD Matter at RHIC, <https://drupal.star.bnl.gov/STAR/starnotes/public/sn0598>.
- [22] NA61/SHINE, L. Turko, Universe **4**, 52 (2018), 1801.06919.
- [23] V. Golovatyuk, V. Kekelidze, V. Kolesnikov, O. Rogachevsky, and A. Sorin, Eur. Phys. J. **A52**, 212 (2016).
- [24] CBM, T. Ablyazimov *et al.*, Eur. Phys. J. **A53**, 60 (2017), 1607.01487.
- [25] J-PARC heavy-ion, H. Sako, JPS Conf. Proc. **8**, 022010 (2015).
- [26] B. Biedron and W. Broniowski, Phys. Rev. **C75**, 054905 (2007), nucl-th/0610083.
- [27] W. Broniowski and B. Biedron, J. Phys. **G35**, 044018 (2008), 0709.0126.
- [28] F. Becattini, J. Cleymans, and J. Strumpfer, PoS **CPOD07**, 012 (2007), 0709.2599.
- [29] F. Becattini and J. Cleymans, J. Phys. **G34**, S959 (2007), hep-ph/0701029.
- [30] J. Brewer, S. Mukherjee, K. Rajagopal, and Y. Yin, (2018), 1804.10215.
- [31] The AFTER@LHC study group, <http://after.in2p3.fr>.
- [32] D. Kikola, A fixed-target programme at the lhc for heavy-ion, hadron, spin and astroparticle physics: After@lhc, Quark Matter 2018, 2018.
- [33] L. Massacrier *et al.*, EPJ Web Conf. **171**, 10001 (2018), 1712.01740.
- [34] L. Massacrier *et al.*, Adv. High Energy Phys. **2015**, 986348 (2015), 1504.05145.
- [35] S. J. Brodsky, F. Fleuret, C. Hadjidakis, and J. P. Lansberg, Phys. Rept. **522**, 239 (2013), 1202.6585.
- [36] D. Kikola *et al.*, Few Body Syst. **58**, 139 (2017), 1702.01546.
- [37] B. Trzeciak *et al.*, Few Body Syst. **58**, 148 (2017), 1703.03726.
- [38] D. Kikola, Adv. High Energy Phys. **2015**, 783134 (2015).
- [39] LHCb, E. Maurice, Fixed-target physics at LHCb, in *5th Large Hadron Collider Physics Conference (LHCP 2017) Shanghai, China, May 15-20, 2017*, 2017, 1708.05184.
- [40] S. A. Bass *et al.*, Prog. Part. Nucl. Phys. **41**, 255 (1998), nucl-th/9803035, [Prog. Part. Nucl. Phys.41,225(1998)].
- [41] M. Bleicher *et al.*, J. Phys. **G25**, 1859 (1999), hep-ph/9909407.
- [42] NA49, H. Appelshauser *et al.*, Phys. Rev. Lett. **82**, 2471 (1999), nucl-ex/9810014.
- [43] BRAHMS, I. C. Arsene *et al.*, Phys. Lett. **B677**, 267 (2009), 0901.0872.
- [44] BRAHMS, F. Videbaek, Nucl. Phys. **A830**, 43C (2009), 0907.4742.
- [45] NA49, T. Anticic *et al.*, Eur. Phys. J. **C65**, 9 (2010), 0904.2708.
- [46] M. Mitrovski, T. Schuster, G. Graf, H. Petersen, and M. Bleicher, Phys. Rev. **C79**, 044901 (2009), 0812.2041.
- [47] V. Ozvenchuk and A. Rybicki, Nucl. Phys. **A973**, 104 (2018), 1711.02963.
- [48] V. Vovchenko, V. V. Begun, and M. I. Gorenstein, Phys. Rev. **C93**, 064906 (2016), 1512.08025.
- [49] V. V. Begun, V. Vovchenko, M. I. Gorenstein, and H. Stoecker, (2018), 1805.01901.
- [50] S. Wheaton and J. Cleymans, Comput. Phys. Commun. **180**, 84 (2009), hep-ph/0407174.
- [51] G. Torrieri *et al.*, Comput. Phys. Commun. **167**, 229 (2005), nucl-th/0404083.
- [52] M. Petran, J. Letessier, J. Rafelski, and G. Torrieri, Comput. Phys. Commun. **185**, 2056 (2014), 1310.5108.
- [53] A. Andronic, P. Braun-Munzinger, K. Redlich, and J. Stachel, (2017), 1710.09425.
- [54] M. Bleicher, J. Steinheimer, and R. Stock, The QCD Phase Diagram from Statistical Model Analysis, pp. 41–64, 2018, 1712.03748.
- [55] S. Chatterjee, A. K. Dash, and B. Mohanty, J. Phys. **G44**, 105106 (2017), 1608.00643.
- [56] D. H. Rischke, M. I. Gorenstein, H. Stoecker, and W. Greiner, Z. Phys. **C51**, 485 (1991).
- [57] G. D. Yen, M. I. Gorenstein, W. Greiner, and S.-N. Yang, Phys. Rev. **C56**, 2210 (1997), nucl-th/9711062.
- [58] G. D. Yen and M. I. Gorenstein, Phys. Rev. **C59**, 2788 (1999), nucl-th/9808012.
- [59] V. Vovchenko, M. I. Gorenstein, and H. Stoecker, Phys. Rev. Lett. **118**, 182301 (2017), 1609.03975.
- [60] J. Letessier, A. Tounsi, U. W. Heinz, J. Sollfrank, and J. Rafelski, Phys. Rev. **D51**, 3408 (1995), hep-ph/9212210.
- [61] STAR, L. Adamczyk *et al.*, Phys. Rev. **C96**, 044904 (2017), 1701.07065.
- [62] ALICE, B. B. Abelev *et al.*, Phys. Lett. **B728**, 216 (2014), 1307.5543, [Erratum: Phys. Lett.B734,409(2014)].
- [63] ALICE, B. Abelev *et al.*, Phys. Rev. **C88**, 044910 (2013), 1303.0737.
- [64] M. Floris, Nucl. Phys. **A931**, 103 (2014), 1408.6403.
- [65] M. Belkacem *et al.*, Phys. Rev. **C58**, 1727 (1998), nucl-th/9804058.
- [66] E. Zabrodin, L. Bravina, M. Bleicher, and H. Stcker, EPJ Web Conf. **126**, 03006 (2016).
- [67] NA49, T. Anticic *et al.*, Phys. Rev. **C94**, 044906 (2016), 1606.04234.
- [68] ALICE, K. Aamodt *et al.*, Eur. Phys. J. **C71**, 1594 (2011), 1012.3257.